


 Cite this: *RSC Adv.*, 2020, 10, 17787

Dependence on co-adsorbed water in the reforming reaction of ethanol on a Rh(111) surface†

 Yu-Yao Hsia,^a Po-Cheng Chien,^b Lu-Hsin Lee,^a Yu-Ling Lai,^c Li-Chung Yu,^c Yao-Jane Hsu,^c Jeng-Han Wang^{*,b} and Meng-Fan Luo^{*,a}

We have studied the reforming reaction of ethanol co-adsorbed with atomic oxygen (O*, * denotes adspecies) and deuterated water (D₂O*) on a Rh(111) surface, with varied surface probe techniques under UHV conditions and with density-functional-theory calculations. Adsorbed ethanol molecules were found to penetrate readily through pre-adsorbed water, even up to eight overlayers, to react at the Rh surface; they decomposed at a probability promoted by the water overlayers. The production probabilities of H₂, CO, CH₂CH₂ and CH₄ continued to increase with co-adsorbed D₂O*, up to two D₂O overlayers, despite separate increasing rates; above two D₂O overlayers, those of H₂, CO and CH₂CH₂ were approximately saturated while that of CH₄ decreased. The increased (or saturated) production probabilities are rationalized with an increased (saturated) concentration of surface hydroxyl (OD*, formed by O* abstracting D from D₂O*), whose intermolecular hydrogen bonding with adsorbed ethanol facilitates proton transfer from ethanol to OD* and thus enhances the reaction probability. The decreasing behavior of CH₄ could also involve the competition for H* with the formation of H₂ and HDO.

Received 3rd March 2020

Accepted 30th April 2020

DOI: 10.1039/d0ra02015j

rsc.li/rsc-advances

1. Introduction

As an efficient approach to produce hydrogen for use in fuel-cells, the reforming reaction of ethanol has drawn considerable attention.¹ Ethanol has advantages of low toxicity, high availability, high hydrogen density and ease of handling and storage; it can be readily extracted from fermentation of biomass like sugarcane and corn.^{2–4} Among various reforming reactions, oxidative steam reforming of ethanol (OSR, C₂H₅OH + (3 – x)H₂O + xO₂ → (6 – 2x)H₂ + 2CO₂) is promising, because its hydrogen yield and exothermicity can be balanced by controlling molar ratios of reagents (ethanol, steam and oxygen).^{4,5} The mechanism of OSR of ethanol has thus been widely investigated. Earlier mechanistic studies find that the reaction is initiated with scission of O–H bond of adsorbed ethanol, forming surface ethoxy (CH₃CH₂O*, * denoting adspecies);^{6–9} either C–H_α or C–H_β bond is sequentially cleaved, producing surface acetaldehyde (CH₃CHO*) and oxametallacycle (CH₂CH₂O*), respectively. The surface acetaldehyde ultimately leads to the production of CH₃CHO, CH₄, CH₃COOH, CO

and CO₂, while the surface oxametallacycle to CH₂CH₂ and CO.^{6,7,10}

The reagent oxygen (molecular) is dissociated into atomic oxygen (O*) on catalyst surfaces; the O* promotes the decomposition probability of ethanol and could also alter the reaction path toward acetaldehyde, as indicated on Rh(100) and Rh(111) surfaces.^{11–13} This alteration highly promotes the production of H₂, along with side products CO, CH₄ and H₂O. With increased oxygen content, the reaction path shifts further to acetate (CH₃COO*) intermediates; the production of H₂ is suppressed but that of CO₂ is highly promoted.¹³ The reagent water (steam) in OSR is typically regarded as another supplier of reagent oxygen or an assistance to the side process—water–gas–shift reaction—of the reforming reaction. Preceding studies on a Rh(111) surface showed comparable effects of hydroxyl (OH*, from dissociated H₂O*) and O*; the OH* further enhanced the reaction probability of ethanol on the Rh surfaces pre-covered with O* but affected little the reaction path.¹³ Nevertheless, how this effect evolves with the quantities of adsorbed water is not clarified. This issue becomes critical as the advantages of OSR depend largely on the molar ratios of its reagents. The present study aims to remedy this lack of knowledge and to shed light on detailed mechanisms.

We have studied the reactions of ethanol co-adsorbed with O* and deuterated water (D₂O*) on a Rh(111) single crystal under ultrahigh vacuum (UHV) conditions. The Rh(111) substrate, as a model system, was chosen because Rh-based catalysts become the most promising catalyst in the reforming reaction^{6,14–19} and (111) facets typically make up a great fraction of the surface of the

^aDepartment of Physics, National Central University, No. 300 Jhongda Road, Jhongli District, Taoyuan 32054, Taiwan. E-mail: mjl28@phy.ncu.edu.tw

^bDepartment of Chemistry, National Taiwan Normal University, No. 88, Sec. 4, Ting-Zhou Road, Taipei, Taiwan. E-mail: jenghan@ntnu.edu.tw

^cNational Synchrotron Radiation Research Center, 101 Hsin-Ann Road, Hsinchu Science Park, Hsinchu 30076, Taiwan

† Electronic supplementary information (ESI) available. See DOI: 10.1039/d0ra02015j



Rh catalysts.^{20–23} Temperature-programmed desorption (TPD) and synchrotron-based photoelectron spectroscopy (PES) were applied to probe the catalyzed reactions, and density-functional-theory (DFT) modelling to illuminate the picture how ethanol interacts with co-adsorbed water. The results show that the reactions of ethanol adsorbed on the Rh surface pre-covered with O* and molecular water proceeded despite adsorbed water increased up to eight overlayers. The reactions persisted as the pre-adsorbed water did not obstruct completely the adsorption of ethanol; besides, the adsorbed ethanol diffused, through exchanging positions with the pre-adsorbed water, toward the Rh surface to react. Furthermore, the decomposition probability was evidently enhanced. The production probabilities of all species, including H₂, CO, CH₂CH₂ and CH₄, were increased with co-adsorbed water, up to two water overlayers; above two water overlayers, those of H₂, CO and CH₂CH₂ exhibited a trend of saturation while that of CH₄ decreased. The behavior is strongly correlated with the concentration of surface OD*. We discussed in detail the mechanisms with our DFT simulations.

2. Methods

2.1 Experimental section

Our experiments were conducted in UHV chambers at a base pressure 4×10^{-10} torr. The Rh(111) single crystal, polished to a roughness <10 nm and an orientation accuracy <0.1°, was purchased from MaTeck GmbH. Before each experiment, alternative cycles of sputtering and subsequent annealing (900 K) were conducted to clean the crystal surface. We confirmed the cleanliness of the crystal surface with surface probe techniques such as low-energy electron diffraction and Auger electron spectroscopy. The crystal was then quenched to desired temperatures for adsorption: molecular oxygen (O₂) at 300 K, deuterated water (D₂O) and ethanol at 120 K. The adsorption was performed with a doser pointing toward the crystal, at a background pressure 5×10^{-8} to 5×10^{-9} torr. Adsorbed O₂ on Rh(111) at 300 K was dissociated into atomic oxygen (O*). The deuterated water (purchased from Merck, 99.8%) was further purified by several freeze–pump–thaw cycles before the adsorption experiments. Their exposures were reported in Langmuir units ($1.0 \text{ L} = 10^{-6}$ torr s). We collected TPD spectra with a quadrupole mass spectrometer (Hiden) to monitor various masses and by ramping the sample at a rate of 3 K s^{-1} ; we shielded and placed the spectrometer near the crystal surface (about 2 mm). The PES experiments were conducted at the BL09A2 beamline (U5 spectroscopy) at National Synchrotron Radiation Research Center in Taiwan.²⁴ The photon beam had a fixed energy 600 eV and was incident normal to the surface; emitted photoelectrons were detected at an angle 58° off from the surface normal. The energy resolution attained 0.1 eV. All PES spectra shown in the current work were normalized to their photon flux. The binding energy (BE) indicated in the spectra is referred to the bulk Rh 3d_{5/2} at 307.1 eV.

2.2 Computational section

Our computations were performed with Vienna *Ab initio* Simulation Package (VASP),^{25–27} a DFT-based computational package

with a 3D periodic boundary condition. The computational level was at GGA-PAW, the generalized gradient approximation²⁸ with Perdew–Wang 1991 formulation²⁹ utilized for the exchange–correlation function. The valence electrons were treated by plane waves with a maximal kinetic energy (cutoff energy) of 600 eV; the core electrons were treated by the cost-effective pseudopotentials implemented in VASP, the projector-augmented wave method (PAW). The integration in the Brillouin-Zone (BZ) was sampled by the Monkhorst–Pack scheme³⁰ with the *k*-point at 0.05×2 ($1/\text{\AA}$) interval in the reciprocal space. For the structural optimizations and energetic calculations of stable adsorptions, we applied quasi-Newton method with an energetic convergence of 1×10^{-4} eV and a gradient convergence of 1×10^{-2} eV \AA^{-1} ; those of transition states were utilized by Nudged Elastic Band method³¹ at the same convergence criterions. The chosen convergence condition has been widely applied in previous studies,^{21,32,33} a convergence test, with a more strict convergence condition (1×10^{-6} eV and 1×10^{-3} eV \AA^{-1}), had also been performed to justify the present calculations.³⁴ The vibrational analysis, with the finite displacement approach at the Γ point,^{35,36} was utilized to confirm the optimized local minimums (without imaginary frequency) and apply zero-point energy (ZPE) corrections on the DFT computed energies.

The Rh(111) surface was constructed with a Rh slab consisting of five layers of 4×4 surface units and equivalent five-layer distant vacuum space to avoid artificial interaction between separate Rh slabs; the bottom two Rh layers were fixed at the computed lattice constants to represent the semi-infinite bulk crystal beneath the surface and the top three layers were free to relax. The adspecies, such as water, ethanol and their fragments, were then placed on the Rh surface for optimization of their adsorption structures and related energies.

3. Results and discussion

3.1 TPD and PES experiments

The reactions of ethanol were monitored primarily with TPD. We compared the TPD spectra from ethanol on Rh(111) pre-covered with O* at 0.08 ML and water at varied coverages to investigate quantitatively the effect of water on the reactions. Adsorbed water molecules alter the OSR reaction of ethanol because they are dissociated into OH*. The dissociation on Rh(111) is largely assisted by pre-adsorbed O*.³⁷ Our previous work showed, in line with other studies,³⁷ that water adsorbed on Rh(111) pre-adsorbed with 0.08 monolayer (ML) O* (denoted as Rh(111)_{O*(0.08 ML)}) yielded a maximal production of OH*,¹³ so we examined the present effect on Rh(111)_{O*(0.08 ML)}. We used deuterated water (D₂O), instead of typical water (H₂O), for our TPD measurements. These isotopic variants behavior similarly, since their adsorption energies, activation energies for dissociation and their interaction with ethanol are determined by their electronic structures, rather than their isotopic properties. Adsorbed D₂O, unlike H₂O, contributed no TPD signals of H₂ and H₂O, two major products from decomposed ethanol on Rh(111)_{O*(0.08 ML)}, but gave clear, separate D₂ (or DH) and D₂O (or DHO) signals. The use of D₂O avoids mixing signals from



different processes and thus permits ready identification of the role of water in the ethanol reaction.

We noted in the series of TPD experiments that adsorbed ethanol penetrated readily through pre-adsorbed water overlayers to react at the $\text{Rh}(111)_{\text{O}^*(0.08 \text{ ML})}$ surface. Fig. 1a shows the D_2O ($m/z = 20$ u) TPD spectra from $\text{Rh}(111)_{\text{O}^*(0.08 \text{ ML})}$ exposed to D_2O of varied amounts (denoted as $\text{Rh}(111)_{\text{D}_2\text{O}^*/\text{O}^*(0.08 \text{ ML})}$). 0.3 L D_2O adsorbed on $\text{Rh}(111)_{\text{O}^*(0.08 \text{ ML})}$ at 120 K gave a single desorption feature around 195 K (the bottom in Fig. 1a), assigned to desorbing sub-monolayer D_2O from the surface. The desorption temperature of the sub-monolayer or monolayer D_2O on $\text{Rh}(111)_{\text{O}^*(0.08 \text{ ML})}$ is higher than that on $\text{Rh}(111)$ (about 170 K, Fig. S1†), because of the formation of a hydrogen-bonded network of D_2O^* and OD^{*37} and also the interaction of D_2O^* with O^* . The desorbing D_2O came from two channels: D_2O^* in the $\text{D}_2\text{O}^*-\text{OD}^*$ hydrogen bonded network and that from disproportionation of OD^* ($2\text{OD}^* \rightarrow \text{D}_2\text{O}^* + \text{O}^*$).³⁷ As the exposure of D_2O increased, the monolayer feature was enhanced; above 1.0 L, the monolayer feature remained similar whereas an additional feature grew about 150 K (top and second in Fig. 1a), which is assigned to the desorption of multilayer D_2O . As the integrated intensity of the D_2O desorption feature increased almost linearly with the exposure and as the desorption feature of 1.0 L D_2O corresponds about to a full monolayer

D_2O , the sticking coefficient of D_2O onto the sample at 120 K is nearly 1; 1.0 L D_2O yielded about a single water overlayer on either $\text{Rh}(111)_{\text{O}^*(0.08 \text{ ML})}$ or $\text{Rh}(111)_{\text{D}_2\text{O}^*/\text{O}^*(0.08 \text{ ML})}$. The D_2O TPD spectra altered significantly when ethanol was adsorbed atop $\text{Rh}(111)_{\text{D}_2\text{O}^*/\text{O}^*(0.08 \text{ ML})}$. For $\text{Rh}(111)_{\text{D}_2\text{O}^*(0.3 \text{ L})/\text{O}^*(0.08 \text{ ML})}$ and $\text{Rh}(111)_{\text{D}_2\text{O}^*(0.5 \text{ L})/\text{O}^*(0.08 \text{ ML})}$ exposed to ethanol (the third and bottom in Fig. 1b), the monolayer feature of D_2O , about 195 K, attenuated, in comparison to those without ethanol (the third and bottom in Fig. 1a), while the multilayer one, about 150 K, emerged. At higher D_2O coverages (the first and second in Fig. 1b), the multilayer feature became obviously enhanced whereas the monolayer one remained smaller than its counterparts without ethanol (the first and second in Fig. 1a). Nevertheless, the integrated intensities of the D_2O lines with and without co-adsorbed ethanol were similar, as plotted in Fig. 1c. The comparison implies that the diminished monolayer D_2O was compensated by the increased multilayer D_2O – a fraction of the first overlayer D_2O on $\text{Rh}(111)$ migrated to the multilayer region and desorbed. The migration was induced because the adsorbed ethanol diffused toward the Rh surface and exchanged position with the underneath D_2O . The involvement of D_2O in the ethanol reaction is reflected on systematically increased DHO desorption signals, which result from surface OD^* (from $\text{D}_2\text{O}^* + \text{O}^* \rightarrow 2\text{OD}^*$, discussed below) abstracting H from ethanol and desorbing as DHO. On such ethanol on $\text{Rh}(111)_{\text{D}_2\text{O}^*/\text{O}^*(0.08 \text{ ML})}$, O^* were entirely consumed and no trace of it was observed with increased temperature,¹³ contrasting ethanol and D_2O separately adsorbed on $\text{Rh}(111)_{\text{O}^*(0.08 \text{ ML})}$.^{13,37} Details are explained in ESI (Fig. S2†) and DFT calculations below.

The TPD spectra for the reaction products of ethanol reveal more the effect of D_2O . Fig. 2a–c show the TPD spectra from 3.0 L ethanol adsorbed on $\text{Rh}(111)_{\text{O}^*(0.08 \text{ ML})}$, $\text{Rh}(111)_{\text{D}_2\text{O}^*(1.0 \text{ L})/\text{O}^*(0.08 \text{ ML})}$ and $\text{Rh}(111)_{\text{D}_2\text{O}^*(2.0 \text{ L})/\text{O}^*(0.08 \text{ ML})}$. The ethanol ($\text{C}_2\text{H}_5\text{OH}$, $m/z = 45$ u) spectra (top lines in Fig. 2a–c) show desorption at 150 and 200 K, corresponding to multilayer and monolayer ethanol respectively. The CO ($m/z = 28$ u), ethylene (CH_2CH_2 , $m/z = 27$ u), H_2O ($m/z = 18$ u), methane (CH_4 , $m/z = 16$ u) and H_2 ($m/z = 2$ u) spectra also show their desorption at various temperatures, the second to the bottom lines in Fig. 2a–c, reflecting the reforming reaction of adsorbed ethanol. Preceding studies argued that adsorbed ethanol on $\text{Rh}(111)$ produced ethoxy readily *via* O–H bond scission and the ethoxy decomposed predominantly *via* C–H_β bond cleavage, which led to formation of oxometallacycle intermediate ($\text{CH}_2\text{CH}_2\text{O}^*$) and further decomposition producing CO, H_2 and surface carbon ultimately;^{12,38,39} on $\text{Rh}(111)_{\text{O}^*}$, the decomposition probability was enhanced and the reaction pathway was largely altered to the one *via* C–H_α bond cleavage, which formed acetaldehyde (CH_3CHO^*) intermediates and promoted the production of H_2 along with the side products of CH_4 and H_2O .^{11,13,39,40} The evident CH_4 and H_2O signals in Fig. 2a confirm the altered reaction pathway; the CH_2CH_2 signals implies the existence of $\text{CH}_2\text{CH}_2\text{O}^*$, whose C–O bond cleavage yields CH_2CH_2 ,⁴⁰ and hence that the channel *via* $\text{CH}_2\text{CH}_2\text{O}^*$ remained active. The observed desorbing species from $\text{Rh}(111)_{\text{D}_2\text{O}^*/\text{O}^*(0.08 \text{ ML})}$ (Fig. 2b and c) were the same as those from $\text{Rh}(111)_{\text{O}^*(0.08 \text{ ML})}$ (Fig. 2a) whereas their intensities differed. Both desorbing multilayer (150

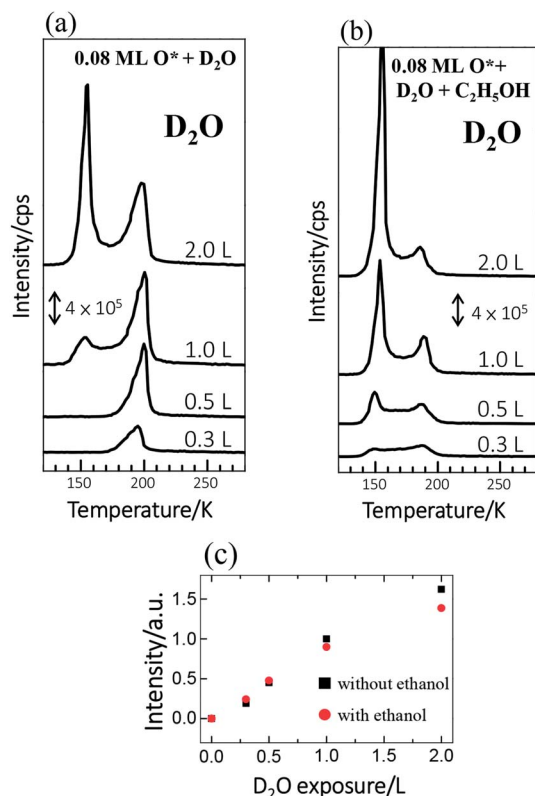


Fig. 1 D_2O TPD spectra from $\text{Rh}(111)_{\text{O}^*(0.08 \text{ ML})}$ exposed to (a) D_2O of varied amounts, as indicated, and to (b) D_2O of varied amounts and subsequently 3.0 L ethanol. (c) Plots the integrated intensities of the D_2O desorption features in (a) and (b) as a function of D_2O exposure; black squares and red spheres denote the data from the sample without and with ethanol, respectively.



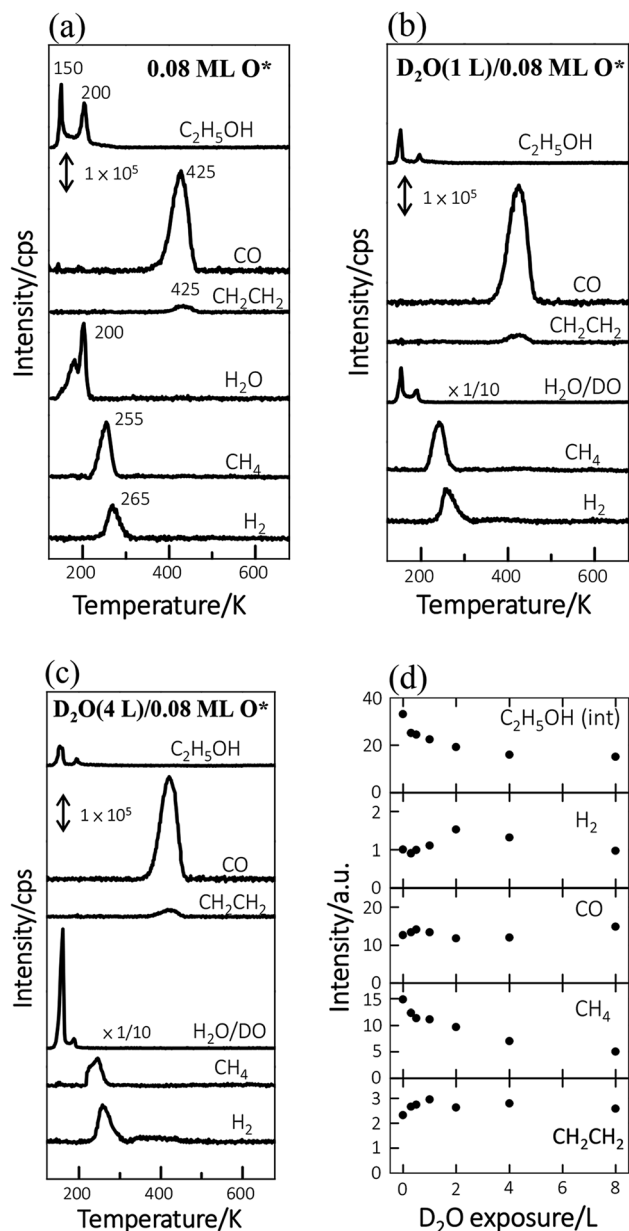


Fig. 2 TPD spectra from 3.0 L ethanol adsorbed on (a) Rh(111)_{O*(0.08 ML)}, (b) Rh(111)_{D₂O*(1.0 L)/O*(0.08 ML)} and (c) Rh(111)_{D₂O*(4.0 L)/O*(0.08 ML)}. (d) Plots the quantities of ethanol_(int) and reaction products, measured with the integrated intensities of the corresponding desorption features, as a function of D₂O exposure. The ethanol_(int) includes those desorbing from and reacting at Rh(111) surface.

K) and monolayer ethanol (200 K), which refer respectively to the ethanol on or in the D₂O–ethanol mixed overlayers and that diffusing to the Rh surface, obviously decreased with increased D₂O (Fig. 2b and c); the sticking coefficient for ethanol onto water overlayers was smaller than that for ethanol onto Rh(111)_{O*(0.08 ML)} (Fig. S3†). The H₂O (*m/z* = 18 u) spectra became highly enhanced (Fig. 2b and c) and resembled the corresponding D₂O spectra (Fig. 1b), as the signals were contributed primarily from adsorbed background H₂O and the cracking pattern of desorbing D₂O (DO, *m/z* = 18 u). The CO, H₂ and CH₂CH₂ signals altered

only a little while the CH₄ ones attenuated systematically with increased D₂O (Fig. 2a–c). The signals of either D₂ or DH were very small (Fig. S4†), indicating few D* and hence limited dissociation of D₂O* into D* and OD*; the OD* was formed predominantly *via* the process D₂O* + O* → 2OD*.

Fig. 2d plots the quantities of the ethanol interacting with Rh(111)_{D₂O*/O*(0.08 ML)} (denoted as ethanol_(int)) and the produced species from ethanol_(int), as a function of D₂O exposure. These quantities were measured with the integrated intensities of their desorption features and had taken into account their various ionization cross-sections. Ethanol_(int) consisted of ethanol adsorbed directly on Rh(111) and also those which adsorbed atop D₂O overlayers and migrated to the D₂O–Rh(111) interface to react or desorb, so contained desorbing and decomposing ethanol at the Rh(111) surface; they were estimated according to desorbing and remaining carbon-related species.⁴¹ The ethanol_(int) decreased when D₂O overlayers increased; it decreased at 8.0 L D₂O (corresponding about to 8.0 water overlayers) to 50% of that on Rh(111)_{O*(0.08 ML)} (top of Fig. 2d). The decrease occurred largely because of a smaller sticking coefficient for ethanol onto D₂O overlayers than that onto Rh(111)_{O*(0.08 ML)}. We note that the ethanol_(int) decreased remarkably between 0.0–2.0 D₂O overlayers but only a little between 2.0–8.0 D₂O overlayers; increasing D₂O above 2.0 overlayers blocked ineffectively the diffusion of adsorbed ethanol toward the Rh(111) surface. Additionally, total adsorbed ethanol (including both multilayer ethanol and ethanol_(int)) decreased with D₂O overlayers in a similar manner (Fig. S3†); the ethanol_(int) made up a great proportion, about 70 ± 5%, of total adsorbed ethanol and the proportion varied insignificantly with increasing D₂O overlayers. The result agrees with the above D₂O TPD spectra (Fig. 1). The produced species responded with increased D₂O in separate manners. The produced CH₄, like ethanol_(int), decreased monotonically with increased D₂O; the H₂ increased at D₂O overlayers ≤ 2.0 L but decreased at higher ones; the CO varied little; the CH₂CH₂ increased with D₂O whereas became saturated above 1.0 L. As ethanol_(int) decreased with the D₂O overlayers, the comparison implies that the probability of the ethanol_(int) undergoing decomposition to produce CO and CH₂CH₂ was enhanced under the D₂O overlayers.

Fig. 3 plots the ratios of the quantities of the produced species to ethanol_(int) as a function of D₂O exposure, to illuminate the altered probability; the red lines are drawn to guide the eyes. The ratios for all products have a similar trend below 2.0 L D₂O exposure—they all increased with D₂O exposure despite of varied increasing rates. Above 2.0 L D₂O exposure, two separate trends are exhibited. For the first kind, the ratio was either saturated, such as H₂ and CH₂CH₂ (first and bottom), or increased slowly, such as CO (second); the other kind, for CH₄, showed a decreasing trend (third). Among these four products, CH₂CH₂ was exclusively contributed from the reaction route *via* CH₂CH₂O* intermediates and CH₄ *via* CH₃CHO* intermediates; the other two products, H₂ and CO, were produced from both the reaction routes. The dissimilar production probabilities of these four products above 2.0 L D₂O exposure are not simply concluded according to the separate reaction routes. Nevertheless, the similar increasing



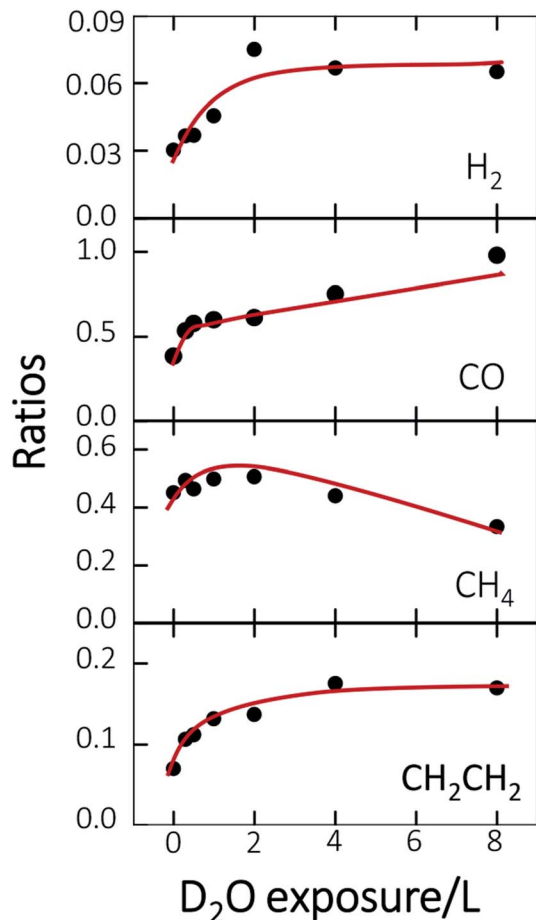


Fig. 3 Ratios of the quantities of reaction products to ethanol_(int) as a function of O* coverage. These quantities were measured with the integrated intensities of the corresponding desorption features. The ethanol_(int) contains those desorbing from and reacting at Rh(111) surface. The red lines are drawn to guide the eyes.

trend below 2.0 L D₂O exposure can be understood through the formation and increased concentration of surface hydroxyl (OH*).

Previous studies indicate that hydroxyl (OH* or OD*) can further enhance the reaction probability of ethanol on Rh surfaces pre-covered with O*, through the intermolecular hydrogen bonding between surface OH* (OD*) with ethanol or its fragments.¹³ The dependence on D₂O coverages of the above production probabilities is strongly correlated with the quantities of OD*. To examine the correlation, we have monitored the production of OH* on Rh(111)_{H₂O*/O*(0.08 ML)} with PES spectra. No substantial difference is anticipated in the formation of OH* on Rh(111)_{H₂O*/O*(0.08 ML)} and OD* on Rh(111)_{D₂O*/O*(0.08 ML)}. Fig. 4a exemplifies the O 1s PES spectra for the produced OH* as a function of H₂O exposure. The bottom panel shows the O 1s line, centered about 529.6 eV, for 0.08 ML O*; upon adsorption of 0.3 L H₂O at 120 K, the O 1s signals for OH* appeared about 530.5 eV (the second from the bottom), in addition to those for H₂O* centered about 532.4 eV.³⁷ The OH* was formed mainly by O* abstracting H from H₂O* (H₂O* + O* → 2OH*). With increased H₂O coverage up to 1.0 L, both H₂O* (light blue fitting curve) and OH* (blue) signals increased while

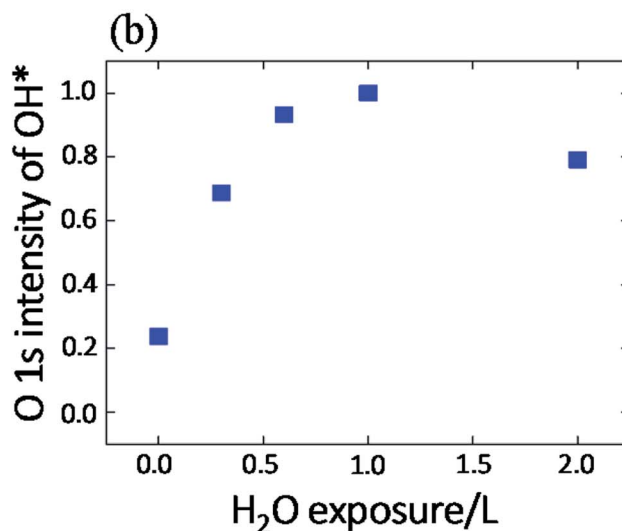
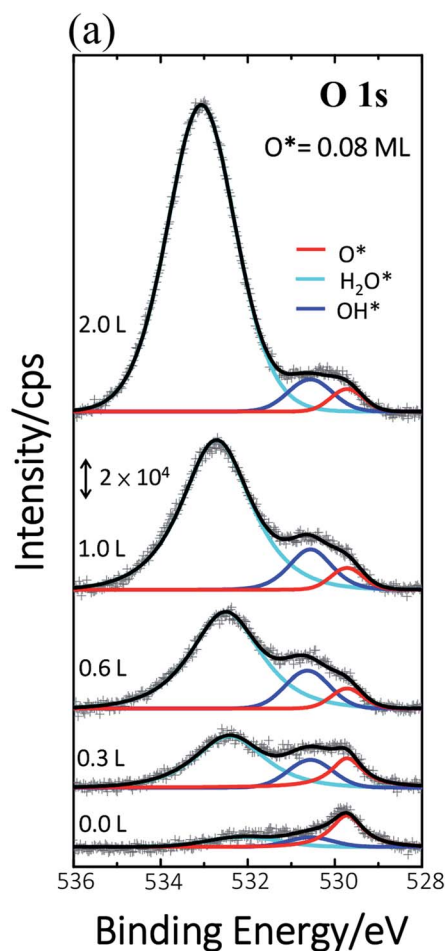


Fig. 4 (a) O 1s spectra for Rh(111)_{O*(0.08 ML)} (bottom) and subsequently exposed to 0.0–2.0 L H₂O, as indicated, at 120 K. The black fitting curves in (a) consist of those for O* (red), OH* (blue) and H₂O* (light blue). (b) Plots the quantities of OH*, measured with the integrated intensities of the fitting curve (blue) for OH*, as a function of H₂O exposure.



O* (red) ones decreased – O* was protonated to OH*; above 1.0 L, the OH* signals became saturated despite the H₂O* ones continued to grow (top). As the observed OH* signals measured the numbers of OH* on the Rh surface, the quantities of OH* increased monotonically with H₂O exposure up to 1.0 L and became saturated above 1.0 L (Fig. 4b). The signal at 2.0 L was slightly attenuated by multilayer water; annealing to 160 K to remove multilayer water restored the OH* signals to about that at 1.0 L. The increased OH* corresponds well to the increased production probabilities of these four products (Fig. 3) below 2.0 L D₂O exposure: the OD* (OH*) promoted the production probabilities. Above 2.0 L D₂O exposure, the OD* was saturated, so the production probabilities of H₂ and CH₂CH₂ were saturated and that of CO increased only slightly; either of them agreed with the saturation of OD* to a great extent. The saturated OD* however could not explain the declining production probability of CH₄ above 2.0 L D₂O exposure. Our analysis based on DFT calculations below gives a more comprehensive picture to understand the evolution of the production probabilities with co-adsorbed D₂O.

3.2 DFT computation and discussion

The experimentally observed phenomena of water and ethanol co-adsorbed on Rh(111) and Rh(111)_{O*} surfaces are mechanistically rationalized according to the schematic plot in Fig. 5. We used H₂O molecule for the computation and compared the results to the above experimental ones with D₂O, because we focused on the properties associated with the electronic structures of Rh(111) surface and adsorbed water (for which H₂O and D₂O are identical), such as desorption energies (E_{des}), reaction

energy (ΔE), activation energies (E_a) and electronic distributions. For water molecularly adsorbed on the surfaces, its E_{des} on Rh(111) surface (top panel, 0.37 eV) is slightly smaller than that on Rh(111)_{O*} surface (middle panel, 0.48 eV), due mainly to a weak hydrogen bond between adsorbed H₂O* and surface O*; the hydrogen bond is evident through the analysis of induced charge that some negative charge is induced on O* (green transparent sphere) and some positive charge on H₂O* (yellow transparent sphere); the computed Bader charge for O* is $-0.90|e|$ and those for O and H of H₂O* are 1.00 and $-1.92|e|$, respectively. The increased E_{des} on Rh(111)_{O*} contributes partly to the increased desorption temperature of first water overlayer (from 170 K to 195 K on Rh(111) surface) in the TPD experiment (Fig. 1a).

The H₂O* on Rh(111)_{O*} surface can further cleave its O–H bond and yield OH*, with energies $\Delta E/E_a = 0.17/0.93$ eV. Upon adsorbing ethanol on the OH* covered surface, the hydrogen bond is readily formed (CH₃CH₂OH*...OH*, middle panel), revealed through the induced charges – positive one (yellow) on the H of CH₃CH₂OH* and negative one (green) on the O of OH*; the computed Bader charges for H and O of OH* are 1.00 and $-1.52|e|$, respectively and that for O of CH₃CH₂OH* is $-1.63|e|$. The hydrogen bond (0.5 eV) stabilizes the adsorption of ethanol and significantly lowers the energies for ethanol dissociation forming CH₃CH₂O* + H₂O* ($\Delta E/E_a = -0.66/0.23$ eV), compared to the dissociation without the hydrogen bond ($-0.19/0.58$).^{9,13} The yielded CH₃CH₂O*, with a much stronger adsorption energy (-2.47 eV), further decomposes (lower panel), while the yielded H₂O* desorbs easily from the surface. As a result, the intermolecular hydrogen bond between co-adsorbed

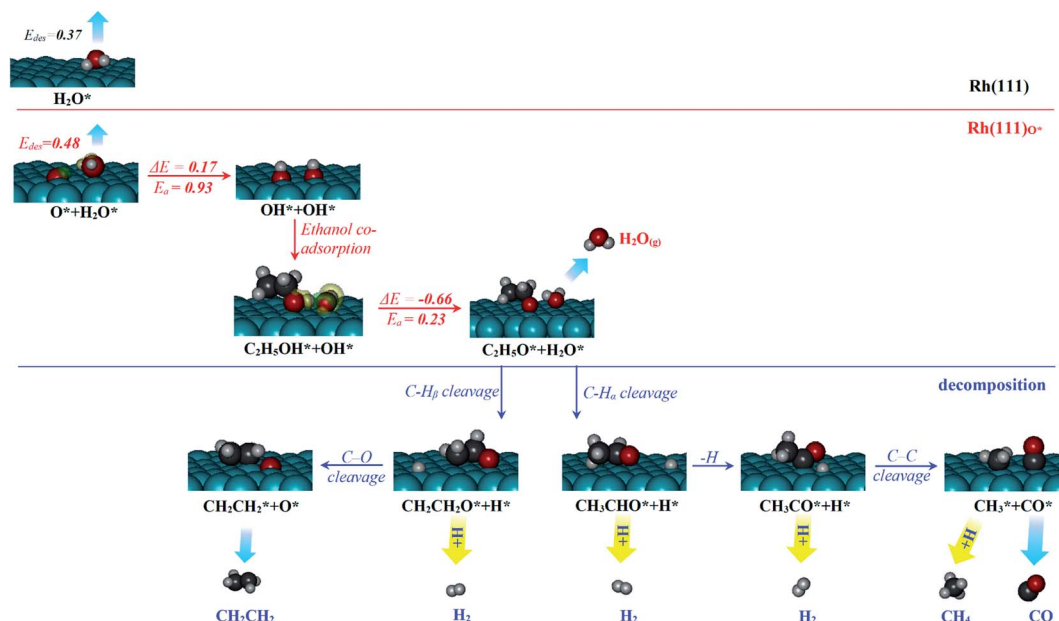


Fig. 5 Schemes of reactions of molecular water, atomic oxygen and ethanol co-adsorbed on a Rh(111) surface. The top panel shows that sole water on the Rh(111) surface has a smaller E_{des} . The middle one shows that water adsorbs on the Rh(111)_{O*} surface with a greater E_{des} and dissociates into OH*, the OH* abstracts H from co-adsorbed ethanol with a small energetic barrier; the green and yellow transparent spheres denotes induced negative and positive charge respectively. The bottom panel shows that the decomposition of CH₃CH₂O* produces CH₂CH₂, H₂, CH₄ and CO.



$\text{CH}_3\text{CH}_2\text{OH}^*$ and OH^* stabilizes the ethanol adsorption and induces a low-barrier and highly exothermic proton transfer process so assists the ethanol dissociation and squeezes water out from the surface. The result explains the TPD observation in Fig. 1b that later adsorbed ethanol exchanged positions with pre-adsorbed surface water so water desorbing from the water multilayer regime increased.

The surface ethoxy ($\text{CH}_3\text{CH}_2\text{O}^*$) is further dissociated on the surface (bottom panel, Fig. 5) through sequences of C–H, C–O and C–C bond cleavages and ultimately produces the products CH_2CH_2 , H_2 , CH_4 and CO , as observed in the TPD spectra (Fig. 2). The detailed energetics and reaction routes are plotted in Fig. S5 in the ESI†; the energetics showed trends similar to those from previous studies (Table S1†).^{20,21,32,33,42} The four products are formed through routes of two kinds, shown with the cyan and yellow arrows in the figure; the measured CH_2CH_2 and CO came from direct desorption of their surface adspecies (cyan arrows), while the measured H_2 and CH_4 from combinative desorption with proton (yellow ones) as their precursors were H^* and CH_3^* , respectively. The quantities of CH_2CH_2 and CO correspond mostly to that of decomposing ethanol (schemes (a) and (b) in Fig. S5†); the increased ratios (production probabilities) of CH_2CH_2 and CO (Fig. 3) thus reflect a promoted decomposition probability of ethanol, by co-adsorbed water (or OD^*). When OD^* was saturated above 2.0 L D_2O exposure, the decomposition probability became (or nearly) saturated so the production probabilities of CH_2CH_2 and CO either remained constant or increased only little.

In contrast, the production of combinatively desorbing CH_4 and H_2 depends to a great extent on the fragments from decomposed ethanol as well as surface H^* (schemes (c) and (d) in Fig. S5†). Surface OH^* (OD^*) from adsorbed water not only enhances ethanol decomposition (by abstracting H of ethanol) but also consumes surface H^* to yield H_2O^* (HDO^*), *via* a moderate energetic reaction ($\Delta E/E_a = -0.01/0.85$ eV). Accordingly, the production of CH_4 or H_2 is balanced between the ethanol decomposition and the availability of H^* . The raised production probabilities of CH_4 and H_2 at smaller water exposure (<2.0 L) correspond largely to a promoted ethanol decomposition, while the decreased (saturated) production probability of CH_4 (H_2) at a greater water exposure (≥ 2.0 L) to not only a saturated probability of ethanol decomposition but also a high consumption rate of H^* (a high ratio of $\text{OH}^*/(\text{OD}^*)$ to $\text{ethanol}_{(\text{int})}$). As the consumption of H^* by OH^* (OD^*) is completed about/below 200 K (Fig. 3), the formation of H_2 and CH_4 competes for the rest H^* . It is noted that the formation of H_2 was more competitive than that of CH_4 even at a smaller water exposure (<2.0 L); with increased water exposure, the H_2 production was increased at a rate much greater than that for the CH_4 production (Fig. 3). The formation of CH_4 was not favored because of an inhomogeneous distribution of CH_3^* . The channel of producing CH_3^* , *via* CH_3CHO^* intermediates, yields less H^* , so less H^* is directly available to CH_3^* ; in contrast, both channels produce H^* so H^* readily finds another H^* nearby to form H_2 . Additionally, a considerable fraction of the precursor CH_3^* underwent dissociation, leading ultimately to formation of surface C^* .^{9,13} Consequently, with limited H^* at a greater water

exposure, the production of H_2 was sustained while that of CH_4 decreased. Our DFT calculations show that an increased OH^* (OD^*) concentration decreases the adsorption energies of CH_3^* , H^* and OH^* but in contrast, enhances the E_a for formation of CH_4 , H_2 and H_2O , which implies equally raised difficulty for their formation. The energetics varied with the OH^* (OD^*) concentration accounts little for the decreased production probability of CH_4 .

4. Conclusion

We have used TPD, PES and DFT calculations to investigate the reactions of ethanol co-adsorbed with atomic oxygen (O^*) and deuterated water (D_2O^*) on a Rh(111) surface under UHV conditions. The results show that adsorbed ethanol penetrated readily through pre-adsorbed water overlayers to react with the Rh surface; for 2.0 L ethanol adsorbed on Rh(111) _{$\text{D}_2\text{O}^*(8.0 \text{ L})/\text{O}^*(0.08 \text{ ML})$} , the $\text{ethanol}_{(\text{int})}$ (which interacted with Rh surface) made up about 75% of total adsorbed ethanol ($\text{ethanol}_{(\text{int})} + \text{ethanol}$ in multilayer regime), a fraction similar to that on Rh(111) _{$\text{O}^*(0.08 \text{ ML})$} , but amounted to 50% of the $\text{ethanol}_{(\text{int})}$ on Rh(111) _{$\text{O}^*(0.08 \text{ ML})$} . The decreased $\text{ethanol}_{(\text{int})}$ with water overlayers results primarily from a smaller sticking coefficient of ethanol onto the water overlayers. In the reaction aspect, the decomposition probability of $\text{ethanol}_{(\text{int})}$ was remarkably enhanced, as the surface OD^* , from $\text{D}_2\text{O}^* + \text{O}^* \rightarrow 2\text{OD}^*$, abstracted readily H from $\text{ethanol}_{(\text{int})}$. The production probabilities of CO , H_2 , CH_2CH_2 and CH_4 were increased in proportion to the concentration of OD^* , despite their increasing rates differed. Above two water overlayers, corresponding to a saturated concentration of OD^* , the production probabilities of CO , H_2 , CH_2CH_2 were about saturated, whereas that of CH_4 was decreased. The atypical behavior of CH_4 could be additionally associated with the availability of H^* . As the formation of CH_4 ($\text{CH}_3^* + \text{H}^* \rightarrow \text{CH}_4$) competes for H^* with that of H_2 ($\text{H}^* + \text{H}^* \rightarrow \text{H}_2$) and HDO ($\text{OD}^* + \text{H}^* \rightarrow \text{HDO}$), both a greater ratio $\text{OD}^*/\text{ethanol}_{(\text{int})}$ at a great water coverages and an inhomogeneous distribution of the precursor CH_3^* could result in the decreased production probability of CH_4 .

Conflicts of interest

There are no conflicts to declare.

Acknowledgements

The work was supported by Ministry of Science and Technology in Taiwan (MOST 107-2113-M-003-008). CPU time at Taiwan's National Center for High-performance Computing (NCHC) and Department of Applied Chemistry in Private Chinese Culture University (PCCU) was greatly appreciated. We thank G. J. Liao for his technical support.

References

- 1 R. M. Navarro, M. A. Peña and J. L. G. Fierro, *Chem. Rev.*, 2007, **107**, 3952–3991.



- 2 G. W. Huber, S. Iborra and A. Corma, *Chem. Rev.*, 2006, **106**, 4044–4098.
- 3 L. V. Mattos, G. Jacobs, B. H. Davis and F. B. Noronha, *Chem. Rev.*, 2012, **112**, 4094–4123.
- 4 P. R. d. l. Piscina and N. Homs, *Chem. Soc. Rev.*, 2008, **37**, 2459–2467.
- 5 M. Ni, D. Y. C. Leung and M. K. H. Leung, *Int. J. Hydrogen Energy*, 2007, **32**, 3238–3247.
- 6 J. Kugai, S. Velu and C. Song, *Catal. Lett.*, 2005, **101**, 255–264.
- 7 A. M. Silva, L. O. O. Costa, A. P. M. G. Barandas, L. E. P. Borges, L. V. Mattos and F. B. Noronha, *Catal. Today*, 2008, **133–135**, 755–761.
- 8 M. Li, W. Guo, R. Jiang, L. Zhao, X. Lu, H. Zhu, D. Fu and H. Shan, *J. Phys. Chem. C*, 2010, **114**, 21493–21503.
- 9 J. H. Wang, C. S. Lee and M. C. Lin, *J. Phys. Chem. C*, 2009, **113**, 6681–6688.
- 10 P. Y. Sheng, A. Yee, G. A. Bowmaker and H. Idriss, *J. Catal.*, 2002, **208**, 393–403.
- 11 B. Caglar, M. Olus Ozbek, J. W. Niemantsverdriet and C. J. Weststrate, *Phys. Chem. Chem. Phys.*, 2016, **18**(43), 30117–30127.
- 12 B. Caglar, J. W. Niemantsverdriet and C. J. Weststrate, *Phys. Chem. Chem. Phys.*, 2016, **18**(34), 23888–23903.
- 13 Y. Y. Hsia, Y. C. Huang, H. S. Zheng, Y. L. Lai, Y. J. Hsu, M. F. Luo and J. H. Wang, *J. Phys. Chem. C*, 2019, **123**, 11649–11661.
- 14 V. Fierro, O. Akdim and C. Mirodatos, *Green Chem.*, 2003, **5**, 20–24.
- 15 G. A. Deluga, J. R. Salge, L. D. Schmidt and X. E. Verykios, *Science*, 2004, **303**, 993–997.
- 16 E. Varga, P. Pusztai, A. Oszkó, K. Baán, A. Erdőhelyi, Z. Kónya and J. Kiss, *Langmuir*, 2016, **32**, 2761–2770.
- 17 M. Tóth, E. Varga, A. Oszkó, K. Baán, J. Kiss and A. Erdőhelyi, *J. Mol. Catal. A: Chem.*, 2016, **411**, 377–387.
- 18 Z. Ferencz, A. Erdőhelyi, K. Baán, A. Oszkó, L. Óvári, Z. Kónya, C. Papp, H. P. Steinrück and J. Kiss, *ACS Catal.*, 2014, **4**, 1205–1218.
- 19 C. C. Hung, S. L. Chen, Y. K. Liao, C. H. Chen and J. H. Wang, *Int. J. Hydrogen Energy*, 2012, **37**, 4955–4966.
- 20 P. Ferrin, D. Simonetti, S. Kandoi, E. Kunkes, J. A. Dumesic, J. K. Nørskov and M. Mavrikakis, *J. Am. Chem. Soc.*, 2009, **131**, 5809–5815.
- 21 Y. Choi and P. Liu, *J. Am. Chem. Soc.*, 2009, **131**, 13054–13061.
- 22 B. N. Zope, D. D. Hibbitts, M. Neurock and R. J. Davis, *Science*, 2010, **330**, 74–78.
- 23 V. Stamenkovic, B. S. Mun, K. J. J. Mayrhofer, P. N. Ross, N. M. Markovic, J. Rossmeisl, J. Greeley and J. K. Nørskov, *Angew. Chem., Int. Ed.*, 2006, **45**, 2897–2901.
- 24 I. H. Hong, T. H. Lee, G. C. Yin, D. H. Wei, J. M. Juang, T. E. Dann, R. Klauser, T. J. Chuang, C. T. Chen and K. L. Tsang, *Nucl. Instrum. Methods Phys. Res., Sect. A*, 2001, **467–468**, 905–908.
- 25 G. Kresse and J. Hafner, *Phys. Rev. B: Condens. Matter Mater. Phys.*, 1994, **49**, 14251–14269.
- 26 G. Kresse and J. Hafner, *Phys. Rev. B: Condens. Matter Mater. Phys.*, 1993, **47**, 558–561.
- 27 G. Kresse and J. Hafner, *Phys. Rev. B: Condens. Matter Mater. Phys.*, 1994, **49**, 14251–14269.
- 28 D. M. Ceperley and B. J. Alder, *Phys. Rev. Lett.*, 1980, **45**, 566–569.
- 29 J. P. Perdew, J. A. Chevary, S. H. Vosko, K. A. Jackson, M. R. Pederson, D. J. Singh and C. Fiolhais, *Phys. Rev. B: Condens. Matter Mater. Phys.*, 1992, **46**, 6671–6687.
- 30 H. J. Monkhorst and J. D. Pack, *Phys. Rev. B: Solid State*, 1976, **13**, 5188–5192.
- 31 G. Mills, H. Jonsson and G. K. Schenter, *Surf. Sci.*, 1995, **324**, 305–337.
- 32 C. Michel, F. Auneau, F.-o. Delbecq and P. Sautet, *ACS Catal.*, 2011, **1**, 1430–1440.
- 33 D. Loffreda, C. Michel, F. Delbecq and P. Sautet, *J. Catal.*, 2013, **308**, 374–385.
- 34 A. A. Gokhale, J. A. Dumesic and M. Mavrikakis, *J. Am. Chem. Soc.*, 2008, **130**, 1402–1414.
- 35 X. Gonze, *Phys. Rev. B: Condens. Matter Mater. Phys.*, 1997, **55**, 10337.
- 36 G. Kresse, J. Furthmüller and J. Hafner, *Europhys. Lett.*, 1995, **32**, 729–734.
- 37 A. Shavorskiy, T. Eralp, E. Ataman, C. Isvoranu, J. Schnadt, J. N. Andersen and G. Held, *J. Chem. Phys.*, 2009, **131**, 214707.
- 38 E. Vesselli, A. Baraldi, G. Comelli, S. Lizzit and R. Rosei, *ChemPhysChem*, 2004, **5**, 1133–1140.
- 39 E. Vesselli, G. Comelli, R. Rosei, S. Freni, F. Frusteri and S. Cavallaro, *Appl. Catal., A*, 2005, **281**, 139–147.
- 40 C. Y. Syu and J. H. Wang, *ChemCatChem*, 2013, **5**, 3164–3174.
- 41 The number of decomposing ethanol molecules are calculated with the carbon atoms of desorbing products and multiplying a factor to include the remaining carbon which is observed from the C 1s signals of photoelectron spectra.
- 42 J. E. Sutton and D. G. Vlachos, *Ind. Eng. Chem. Res.*, 2015, **54**, 4213–4225.

